HAL
open science

The effect of air velocity on slugs in a confined channel

Hella Adouni, Yoldoss Chouari, Wassim Kriaa, Hervé Bournot

To cite this version:

Hella Adouni, Yoldoss Chouari, Wassim Kriaa, Hervé Bournot. The effect of air velocity on slugs in a confined channel. Flow Measurement and Instrumentation, 2021, 81, pp.102013. 10.1016/j.flowmeasinst.2021.102013 . hal-03654964

HAL Id: hal-03654964

https://amu.hal.science/hal-03654964v1

Submitted on 29 Apr 2022

HAL is a multi-disciplinary open access archive for the deposit and dissemination of scientific research documents, whether they are published or not. The documents may come from teaching and research institutions in France or abroad, or from public or private research centers.

L'archive ouverte pluridisciplinaire **HAL**, est destinée au dépôt et à la diffusion de documents scientifiques de niveau recherche, publiés ou non, émanant des établissements d'enseignement et de recherche français ou étrangers, des laboratoires publics ou privés.

The effect of air velocity on slugs in a confined channel

Hella Adouni[a], Yoldoss Chouari[a], Wassim Kriaa[a], Hervé Bournot[b]
[a]*LTTPI, National Engineering School of Monastir, University of Monastir, Tunisia*
[b]*Aix Marseille University, CNRS, IUSTI, Marseille, France*

Abstract: The present work focuses on the study of slugs occurring in a two-phase flow of a confined rectangular channel: conditions of appearance and effect on the flow behavior. Three-dimensional numerical simulations have been carried out to examine the effect of superficial air velocity on flow behavior. The Volume Of Fluid model (VOF) is used to track the air-water interface. Validation of the numerical model is obtained by comparing the results of the simulated axial velocity with experimental data determined using the Laser Doppler Anemometry (LDA) technique. The numerical results revealed that for a fixed water level and superficial water velocity, higher superficial air velocities generate a slug flow that causes channel blockage. The position of these slugs and the timing of their occurrence were correlated in terms of air and water superficial velocities.

Key-words: two-phase flow, slug flow, confined channel, sewer system, VOF method

Nomenclature

Notation

A	Constant
L	Channel length, m
H	Channel height, m
H_L	Water level, m
T	Time, s
t_s	Slug occurrence time, s
X	Coordinate in direction of flow
Y	Coordinate in direction of flow
X_s	Slug occurrence position, m
V^s	Superficial velocity, m/s
A	Flow cross-sectional area, m²
u	Mean velocity, m/s
U_x	Axial velocity, m/s
P	Static Pressure, Pa
I	Turbulent intensity
G_k	generation of turbulent energy
k	Turbulent kinetic energy, m²s²
Re_{air}	Air Reynolds number, $Re_{air} = \frac{\rho_{air}\, D_{air}\, u_{air}}{\mu_{air}}$
Re_{water}	Water Reynolds number, $Re_{water} = \frac{\rho_{water}\, D_{water}\, u_{water}}{\mu_{water}}$
D_{air}	Hydraulic Diameter, m $D_{air} = \frac{4\, A_{air}}{S_{air} + S_i}$
D_{water}	Hydraulic Diameter, m $D_{water} = \frac{4\, A_{water}}{S_{water}}$

Greek Symbols

μ	Dynamic Viscosity (Kg s^{-1} m^{-1})
μ_t	Turbulent dynamic viscosity (Kg s^{-1} m^{-1})
δ	Kronecker delta
α	Volume fraction
τ_{ij}	Stress tensor (Kg s^{-2} m^{-1})
ε	Dissipation rate of turbulent kinetic energy (m^2s^{-3})
ρ	Density (kg m^{-3})

Subscripts

i	Air water interface
s	slug

S Perimeter, m

1. Introduction

The increased awareness of environmental pollution and the considerable efforts deployed to reduce it have made the study of two-phase flows a very important concern. Two-phase flows are very common in hydraulic systems such as pumping stations, hydropower plants and sewer systems, etc. This study focuses on the dynamic of two-phase flow in horizontal confined channels of sewerage systems that may be a major source of pollution. This is a topical issue in view of the accidents that may occur due to recent climate changes; the changing weather patterns lead to an increase in the frequency and intensity of precipitation, which affects the infrastructure of drainage systems. The evacuation capacities of rainwater systems will be exceeded by the recurrence of intense and/or extended rainfall events. In this regard, the lack of understanding and control of the characteristic parameters of two-phase flows in drainage systems would be threatening.

During the process of evacuating waste water at discharge points, the most common problem encountered is air entrapment [1], [2], [11], [12], [3]–[10]. This phenomenon occurs for many reasons, including the transition from the stratified smooth flow regime to the surcharged flow regime [1] and the insufficient ventilation of the channel as a result of insufficient aeration[2]–[4] . The compression of trapped air pockets generates pressure variations that can threaten the channel infrastructure[5]–[8]. These pressurized air pockets create a force on the water surface, which produces a water lift that causes the pipe to become blocked in some cases, and the water to drain through manholes and ventilation shafts in other cases[9]. During rainy events, the rapid filling of drainage system forces the transition to surcharged flow that causes undesired consequences such as: street and basement flooding, severe infrastructure damage, geysers, rupture of drainage tunnel and violent expulsion of manholes. There are a range of published works that highlight the harmful consequences of the existence of transient flow inside drainage systems. In the western part of Mexico City, heavy rains has caused the rupture of drainage tunnel which resulted in three deaths, flooding of wastewater and severe infrastructure damage [13]. Destructive geysering has happened in the Bonnie Doon area of Edmonton, Canada drainage system and in the Minneapolis storm water tunnel system [6], [11]. All these issues show the crucial need to understand confined two phase flows and the importance of mastering the characteristic parameters of these flows in order to anticipate and

avoid problems that may occur. To find a remedy to this issue, a study allowing the understanding of two-phase flows in confined horizontal channels is essential.

Many researchers have experimentally investigated the internal two phase flow [14], [15], [24]–[31], [16]–[23]. Hudaya et al. [14] studied the interfacial characteristics of a stratified wavy air-water flow. Experiments were conducted in a horizontal pipe with a diameter of 26 mm. The study shows that the average liquid holdup decreases with increasing superficial gas velocity. In addition, the wave velocity increases as the superficial gas velocity increases. Dinaryanto et al. [15] focused on the slug flow regime. Tests were conducted in a pipe of 26 mm inner diameter. The slug initiation mechanisms were explained by visual observation using two video cameras. These were wave coalescence, wave growth mechanism and large disturbance waves. Kong et al.[16] conducted an experimental study of air-water flow in different sizes of horizontal pipes, small (38.1 mm) and large (101.6 mm). The study shows that increasing pipe size has a clear effect on flow dynamics. In addition to pipe size, the geometry of the pipe can also be an important factor affecting the transition limits from one regime to another. Hamam et al. [1] have shown that gravity flow in a circular pipe is more unstable than in a rectangular pipe. Although several two-phase flow studies have been conducted on circular pipes, few studies have been carried out on rectangular channels[17]–[19]. Vallee et al. [18] worked on an air-water flow in a large rectangular channel (height x width = 250 x 50 mm2). Measurements were carried out using a high-speed video camera and were complemented by simultaneous dynamic pressure measurements. They revealed that the rapid increase in pressure is related to the length of the slugs. In addition to the experimental studies, several numerical studies were carried out on two-phase flows[32]–[41]. De Schepper et al. [32] numerically reproduced the two-phase air-water flow regimes in a pipe with a diameter of 80 mm. The VOF multiphase flow model was used. They showed that CFD is a useful tool for reproducing two-phase flow regimes and that the VOF model is well suited to accurately follow the geometry of the interface. Dabirian et al. [33] numerically studied an air-water flow in a horizontal pipe with an inner diameter D=96 mm. They analyzed several characteristic flow parameters such as liquid level, shear stress, velocity profile...etc. The results obtained using the VOF model agree well with the experimental data, especially for low gas velocities. Other research[34]–[36], [41] examined the ability of numerical models to predict the development and characteristics of intermittent flows (slug flow and plug flow). Nasrfard et al. [34] simulated two-phase flow in a 14.4 m long pipe with an inside diameter of 54 mm. They concluded that using the VOF model, the formation and

propagation of the slug flow regime along horizontal circular pipes is successfully described and validated against the experimental results. Costa et al. [35] worked on a horizontal pipe with an inside diameter of 26 mm using the VOF method. Parameters such as slug velocity and slug length were in good agreement with the experimental results, with relative errors of less than 8% for the slug velocity. Following up on the same challenge, W.PAO et al. [36] examined the ability of CFD to predict slug development in horizontal pipes with a diameter D=74 mm and length L = 8m. By comparing the numerical results with the experimental data, the slug flow regime was successfully described. They added that the VOF technique perfectly describes all the phenomena of this regime in horizontal pipes. All of these numerical studies demonstrated the efficiency of the model (VOF) in reproducing two-phase flow regimes. However, all the studies have been subject to characterization of two-phase flows, but none of them, to our knowledge, has accurately examined the conditions of slug occurrence causing blockage in confined channels and their effect on the characteristic parameters of the flow.

The objective of this work is to numerically discuss the behavior of two-phase flow in a confined horizontal rectangular channel under the effect of the variation of the superficial air velocity. The geometrical and dynamical conditions adopted are in accordance with the test bench of the IUSTI laboratory of the University of Aix Marseille on which we carried out the experimental measurements using the LDA technique. The experiments also provided us with reference data to validate the simulated model. In this study, we are mainly interested in the slug flow regime that can occur in these channels: conditions of occurrence and effect on the flow. Numerical correlations capable of predicting the time t_s and position X_s of slugs are presented.

2. Experimental setup

The experiments were carried out at the IUSTI laboratory of the University of Aix Marseille. Figs. 1(a) and (b) show a photograph of the experimental setup. It consists of a rectangular confined and horizontal channel (height x width = 150 x 75 mm²) with a length L equal to 5 m and whose walls are made of acrylic glass. The channel is mounted between two tanks, the upstream part is preceded by a tank with a capacity of $77.5\ 10^{-3}\ m^3$, and in order to work in a closed circuit, downstream of the channel, the water flows into the second tank with a capacity equal to $31\ 10^{-3}\ m^3$. The water is redirected to the upstream tank through a pipe with a diameter of 35 mm. The water flow is controlled by a pump with a maximum flow rate

equal to 2.84 l/s. The adjustment of the water height is ensured by a valve mounted on the supply pipe. The position of the free surface is taken with a cathetometer with an accuracy of 0.5 mm and is measured in relation to the ceiling of the channel. The air is introduced by a double suction centrifugal fan with forward curved blades and a speed of between 1150 and 1550 rpm. In order to ensure a good distribution of the air flow inside the channel, a connecting duct links the channel to the fan. The air velocity in the channel is controlled by a power unit and the initial air velocity cross section profile is measured with a hot wire anemometer. Water velocity measurements were made using a laser Doppler anemometer. The two fluids flow parallel and in the same direction and are introduced at room temperature. In order to locate the different flows and to scale the different characteristics, a Cartesian coordinate system is introduced and its origin is placed at the bottom and at the inlet of the channel. Two experiments were carried out for two different water levels. The velocity measurements were carried out at points distributed over the height of the channel in the median plane at y=0.02m from the bottom to 0.145 m for both experiments. Table 1 summarizes the values of the hydrodynamic parameters characterizing the experiments.

Table 1 the hydrodynamic parameters characterizing the experiments

	Height [m]		**Velocity [m/s]**		**Density [Kg/m^3]**	
	H_L	H_{air}	V^s_{water}	V^s_{air}	ρ_{water}	ρ_{air}
Experiment 1	0.032	0.118	0.1	2.5	998.2	1.225
Experiment 2	0.056	0.094	0.16	5		

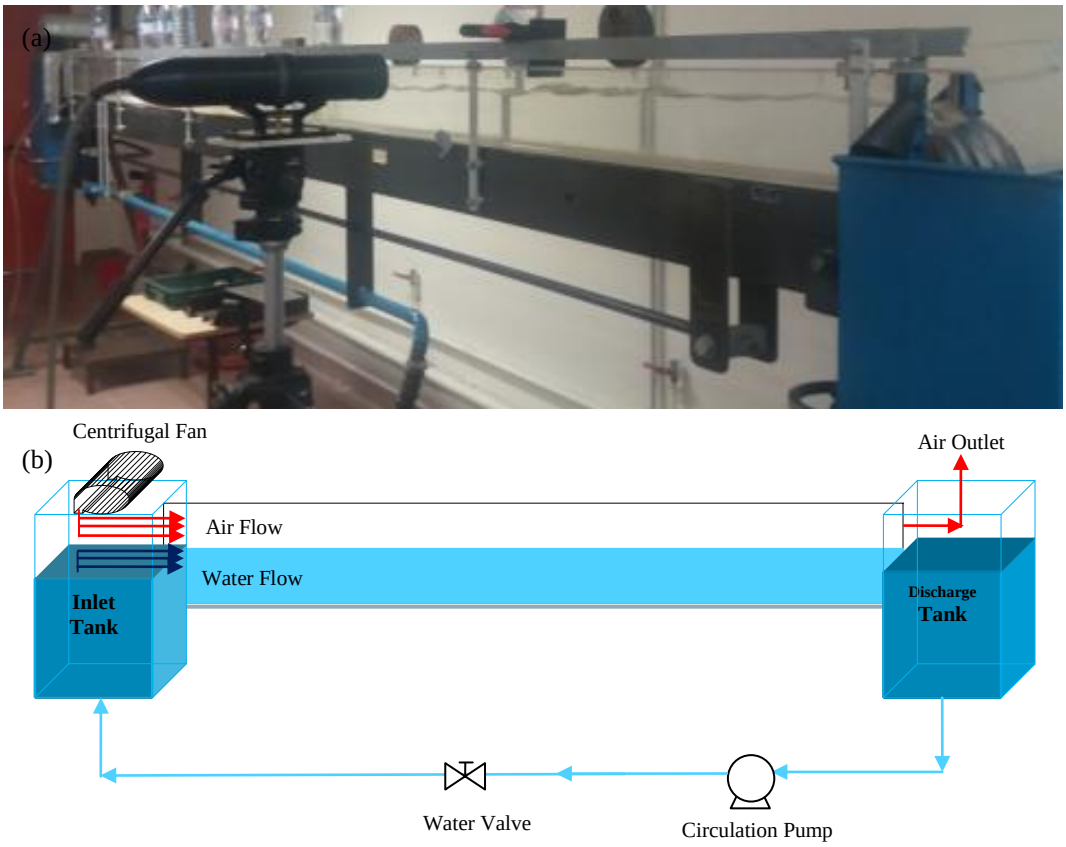

Fig.1. a. Photograph of the experimental setup of the IUSTI, b. Schematic diagram of the experimental setup

3. Computational setup

3.1 Studied configuration and generated mesh grid

The rectangular and confined channel of the IUSTI presented in paragraph 2 has been simulated. The adopted mesh is hexahedral (Fig. 2(a)). It is dense at the interface between the two fluids (Fig. 2(c)) and in the areas close to the channel walls (Fig. 2(b)). Several mesh volumes constituted of a number of cells between 930,000 and 1,800,000 were tested. The sensitivity of the results to the mesh size will be presented in the paragraph 4.1.

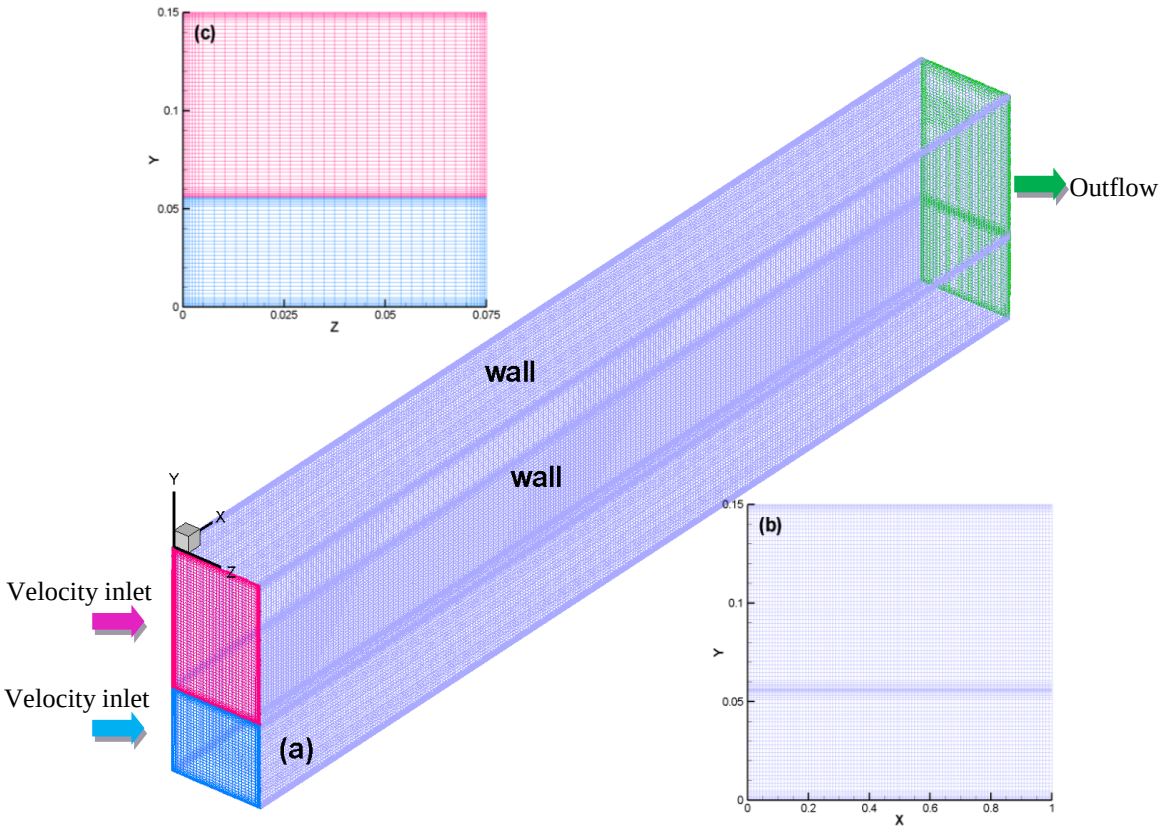

Fig.2: a. Generated mesh grid for the channel, b. Mesh grid of the channel wall, c. Mesh grid of the channel inlet (air inlet and water inlet section)

3.2 Assumptions

For all the simulations, the following assumptions will be considered:

- The flow is composed of two fluids (air and water) assumed to be Newtonian, immiscible and incompressible (Mach<0.3) [42],
- The flow is unsteady and isothermal,
- The effect of surface tension is taken into account,
- The flow is supposed to be turbulent (Re_{water} = 21,046 > 2,000 ; Re_{air} = 5,712 > 2,000) [43].

3.3 Governing Equations

The Equations governing the two-phase air-water flow studied are the Navier-Stokes Equations. Taking into account the above assumptions, the mass conservation Eqs.1, and the momentum conservation Eqs.2 are written as follows [44]:

$$\frac{\partial \rho}{\partial t} + \frac{\partial \rho u_i}{\partial x_i} = 0 \tag{1}$$

$$\frac{\partial \rho u_i}{\partial t} + \frac{\partial \rho u_i u_j}{\partial x_j} = -\frac{\partial P}{\partial x_i} + \frac{\partial \tau_{ij}}{\partial x_j} + \rho f_i \tag{2}$$

With

$$\tau_{ij} = \mu \left(\frac{\partial u_i}{\partial x_j} + \frac{\partial u_j}{\partial x_i}\right) - \frac{2}{3}\, \mu\, \delta_{ij} \frac{\partial u_l}{\partial x_l} \quad ; \ (l = i, l = j) \tag{3}$$

Where, u_i, u_j, u_l are velocity components along the axis of the Cartesian system (x_i, x_j, x_l) with (i, j, l = 1, 2, 3), respectively. Also, t is time, ρ is fluid density, P is pressure, τ_{ij} is stress tensor, δ_{ij} is Kronnecker delta, f_i are volume forces and μ is dynamic viscosity.

For the closure of Eqs. (1)-(2), we considered three turbulence models: the standard $\boldsymbol{k-\varepsilon}$ model, the RNG $\boldsymbol{k-\varepsilon}$ model and the realizable $\boldsymbol{k-\varepsilon}$ model. These models are based on the Equations of the turbulent kinetic energy $\boldsymbol{k}$ and the dissipation rate $\boldsymbol{\varepsilon}$. The RNG $\boldsymbol{k-\varepsilon}$ model is recommended for flows involving recirculation and interface curvature [45]–[49]. The turbulent kinetic energy $\boldsymbol{k}$ and the dissipation rate $\boldsymbol{\varepsilon}$ Equations for this model can be written in the following way [50]:

$$\frac{\partial}{\partial t}(\rho k) + \frac{\partial}{\partial x_i}(\rho k u_i) = \frac{\partial}{\partial x_j}\left[\left(\mu + \frac{\mu_t}{\sigma_k}\right)\frac{\partial k}{\partial x_j}\right] + G_k - \rho\varepsilon \tag{4}$$

Where, μ_t is turbulent dynamic viscosity, σ_k is empirical constant and G_k is the turbulent energy generation term.

$$\frac{\partial}{\partial t}(\rho \varepsilon) + \frac{\partial}{\partial x_i}(\rho \varepsilon u_i) = \frac{\partial}{\partial x_j}\left[\left(\mu + \frac{\mu_t}{\sigma_\varepsilon}\right)\frac{\partial \varepsilon}{\partial x_j}\right] + C_{1\varepsilon}^{*}\, \frac{\varepsilon}{k} G_k - C_{2\varepsilon}\, \rho \frac{\varepsilon^2}{k} \tag{5}$$

With

$$\mu_t = C_\mu\, \rho \frac{k^2}{\varepsilon} \tag{6}$$

$$G_k = \mu_t \left(\frac{\partial u_i}{\partial x_j} + \frac{\partial u_j}{\partial x_i}\right) \frac{\partial u_i}{\partial x_j} \tag{7}$$

$$C_{1\varepsilon}^{*} = C_{1\varepsilon} - \frac{\eta\,(1 - {}^{\eta}/_{\eta_0})}{1 + \beta\eta^3} \tag{8}$$

$$\eta = \sqrt{\frac{G_k}{\rho C_{\mu\varepsilon}}} \tag{9}$$

Where, C_μ, $C_{1\varepsilon}$, $C_{2\varepsilon}$, β, σ_k, σ_ε and η_0 are empirical constants of the RNG $k-\varepsilon$ model and their values are given in Table 2.

Table 2: empirical constants of the RNG $k-\varepsilon$ model [50]

C_μ	$C_{1\varepsilon}$	$C_{2\varepsilon}$	σ_k	σ_ε	η_0	β
0.085	1.42	1.68	0.717	0.717	4.38	0.012

The transport Equations of the turbulent kinetic energy $\boldsymbol{k}$ and the dissipation rate $\boldsymbol{\varepsilon}$ of the standard $\boldsymbol{k}-\boldsymbol{\varepsilon}$ model and the realizable $\boldsymbol{k}-\boldsymbol{\varepsilon}$ model are available respectively in the references [51] and [52].

To predict the air-water interface, the Volume Of Fluid (VOF) model was chosen. This model is based on the calculation of the volume fraction allowing the localization of the interface between the two immiscible fluids. In the following, the different Equations used by this model to simulate the air-water interface are given. The idea is to calculate the corresponding volume fraction of air and water at each iteration. The volume fraction α for a phase q is calculated from the following conservation Equations. [53] :

$$\frac{\partial}{\partial t}\left(\alpha_q \rho_q\right) + \nabla.\left(\alpha_q \rho_q \vec{u}_q\right) = 0 \tag{10}$$

With

$$\sum_{q=1}^{n} \alpha_q = 1 \tag{11}$$

The density and the viscosity of the fluid in each cell are calculated as follows [53]:

$$\rho = \sum \alpha_q \rho_q \tag{12}$$

$$\mu = \sum \alpha_q \mu_q \tag{13}$$

3.4 Initial conditions

The starting pattern present at time t=0s correspond to the a stratified smooth flow for a superficial velocity of air equal to 0.6 m/s and water equal to 0.16 m/s. Transient simulations

are then run for higher air and water velocities (see Table 3). The operating pressure for all simulations is set at 101,325 Pa.

3.5 Boundary conditions

The boundary conditions are illustrated in Fig. 2 and summarized in Table 3. The turbulent kinetic energy is calculated from turbulent intensity I as follows [54]:

$$K = \frac{3}{2}\,(u\,I)^2 \tag{14}$$

With

$$I = 0.16\,(\,Re^{-1/8}\,) \tag{15}$$

The energy dissipation rate is calculated using the turbulence scale length l as follows[54]:

$$\epsilon = C_u^{3/4}\frac{k^{3/2}}{l} \tag{16}$$

For internal flows in non-cylindrical channels, the turbulence scale length l is based on the hydraulic diameter D by the following correlation [54]:

$$l = 0.07\,D \tag{17}$$

Table 3: Boundary conditions

Boundary Conditions		H_L = 0.21 H		H_L = 0.37 H	
		Velocity (m/s)	**Turbulence K (m^2s^2) ε (m^2s^{-3})**	**Velocity (m/s)**	**Turbulence K (m^2s^2) ε (m^2s^{-3})**
Air inlet	« Velocity inlet »	V^s_{air} = 2.5	K =0.060 ε =0.3763	0.6< V^s_{air}<13	0.0082<K<1.6565 0.0209<ε<59.9859
Water inlet	« Velocity inlet »	V^s_{water} = 0.10	K=0.0015 ε =0.0031	0.16<V^s_{water}<0.3	0.0011<K<0.0032 0.0014<ε<0.0067
Channel walls	« Wall »	U = V = W =0	K = 0 ; ε =0	U = V = W =0	K = 0 ; ε =0
Outlet	« Outflow »	$\frac{\partial U}{\partial x} = \frac{\partial V}{\partial x} = \frac{\partial W}{\partial x} = 0$	$\frac{\partial k}{\partial x} = \frac{\partial \varepsilon}{\partial x} = 0$	$\frac{\partial U}{\partial x} = \frac{\partial V}{\partial x} = \frac{\partial W}{\partial x} = 0$	$\frac{\partial k}{\partial x} = \frac{\partial \varepsilon}{\partial x} = 0$

Where U, V, W are velocities according to x, y, z, respectively.

3.6 Numerical method

Numerical simulations of the two-phase air-water flow were performed using the commercial CFD code Fluent. Due to the behavior of the flow, transient calculations were implemented with a variable time step having a minimum value of 10^{-5}s. This method makes

it possible to set a constant CFL flow number (CFL=2), and thus to have a stable solution. The PISO algorithm (Pressure-Implicit with Splitting of Operators) was used for the pressure-velocity coupling. The transport Equations were discretized using a second order upwind scheme. The geo-reconstruction scheme (Geo-reconstruct) was used for the discretization of the transport Equation of the volume fraction. The residuals of the various parameters contributing to the convergence criterion were set at 10^{-3}.

4. Results and discussion

4.1 Study of the sensitivity of the results to the grid size

In order to study the sensitivity of the numerical results to the grid size, the channel was simulated using the Standard k-ε model for the three grid densities cases considered in Table 4. The boundary conditions are those given in Table 3 (H_L=0.21 H).

Table 4: Characteristics of the three meshes tested

	Mesh1	Mesh2	Mesh3
Total cells number	930,000	1,314,000	1,800,000

Fig. 3 shows the vertical profiles (according to y) of the axial velocity U_x at x = 41 D in the median plane. It is noted that mesh1 gives a completely different velocity profile from the profiles obtained using meshes 2 and 3. The latter give similar results. Thus, to gain in computing time, the grid size chosen is mesh2 consisting of 1,314,000 cells.

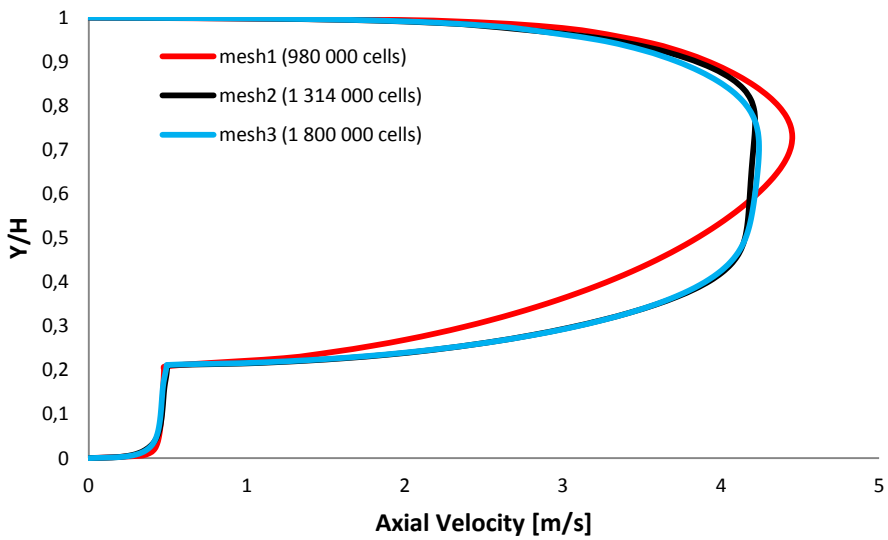

Fig.3: Vertical profiles of the axial velocity U_x at x = 41 D in the median plane for H_L = 0.21 H.

4.2 Study of the turbulence model validity

In order to choose the best turbulence model, simulations were carried out with the first order models: The Standard K-ε model, the RNG K- ε model and the Realizable K- ε model for two cases (H_L = 0.21 H et H_L = 0.37 H) as already mentioned in Table 1.

Fig. 4 shows the vertical profiles of the axial velocity U_x for x = 41 D in the median plan at a fixed water level (H_L = 0.21 H). As can be seen, the shape of the computed velocity profiles for the Realizable K- ε model presents a different result from the other two models. It overestimates the maximum air velocity. However RNG K- ε model and Standard K- ε model gave very similar results and are in good agreement with the experimental results.

Fig. 5 shows the vertical profiles of the axial velocity for x = 41 D in the median plan at a fixed water level (H_L = 0.37 H). In this case, it is noted that the more the air velocity increases the more the results given by the K-ε Standard gets away from the experimental ones, unlike the K-ε RNG model, which maintains its accuracy. Thus, the choice was made for the K-ε RNG model.

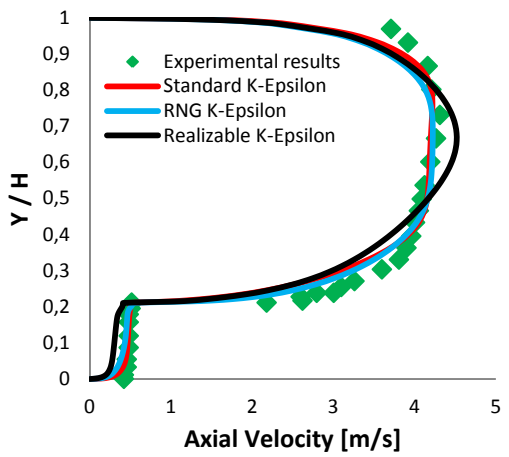

Fig.4: Vertical profiles of the axial velocity U_x for x = 41 D in the median plane at HL = 0.21 H

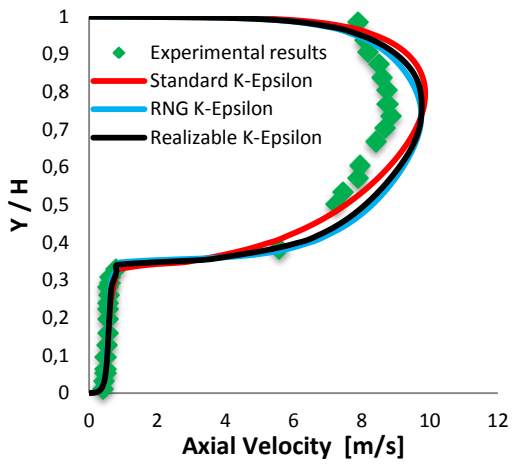

Fig.5: Vertical profiles of the axial velocity for x = 41 D in the median plan at HL = 0.37 H

4.3 Study of the superficial air velocity effect

In order to investigate the effect of air on the flow pattern and to identify the critical superficial air velocity that causes interfacial disturbance leading to a slug creation and a blockage in the channel, we have simulated 19 cases keeping the superficial water velocity constant at V^S_{water} = 0.16m/s for a range of superficial air velocity from 1m/s to 13m/s. Four cases, we judge significant, are presented in this section: V^s_{air} = 1, 5, 8.4 and 10 m/s.

Fig. 6 illustrates the evolution of the air-water interface under the effect of superficial air velocity at t = 0.4s for the 4 mentioned cases. t = 0.4s represents the time at which the slug is

clearly observed for V^S_{air} = 10 m/s. For low superficial air velocities (case 1: V^s_{air} = 1 m/s and case 2: V^s_{air} = 5 m/s), the interface remains smooth and no waves are observed. This regime is called stratified smooth flow. Then, for medium superficial air velocities (case 3: V^s_{air} = 8.4 m/s), there is extra air energy transferred to water which manifests interface instability and the wavy flow occurs. All these cases did not show slug flow at t = 0.4s. Moreover, for higher superficial air velocities (V^s_{air} = 10 m/s), large amplitude waves appear, which significantly modifies the shape of the interface causing complicated flow pattern behaviour. Interface instability brings on transition to slug flow which results in a complete blockage of the air flow downstream the channel.

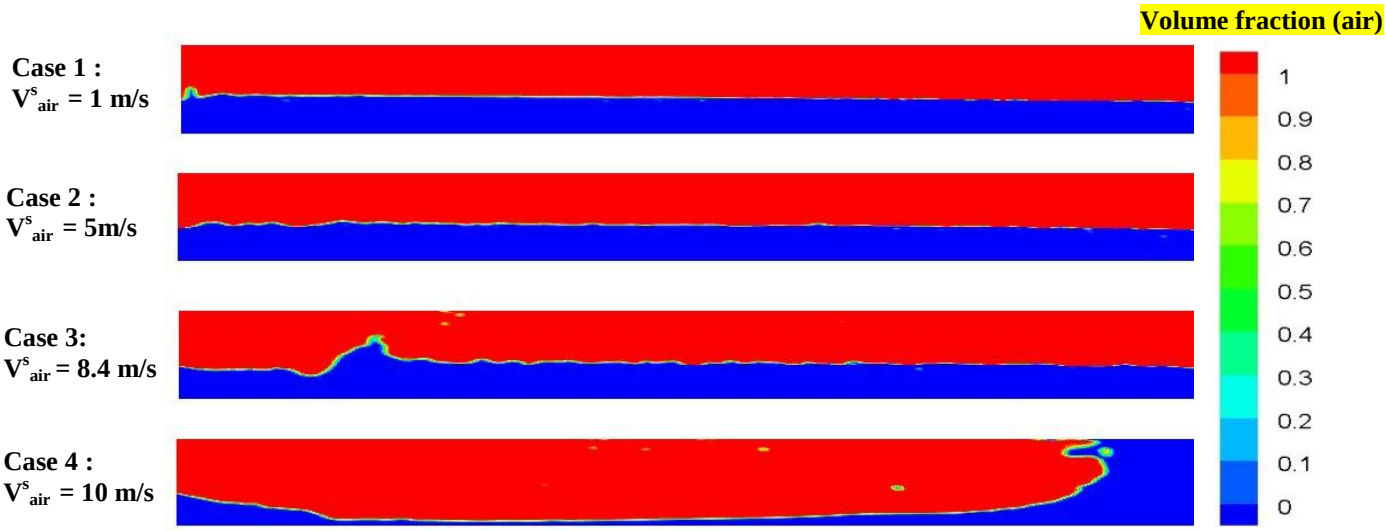

Fig.6: Contours of volume fraction in the median plane for air-water flow for different superficial air velocities at t = 0.4 s

Fig. 7 shows the vertical profiles of the axial velocity U_x for x = 15 D in the median plan for different superficial air velocities (V^S_{air} = 1, 5, 8.4, and 10 m/s) at t=0.4s. For low and medium superficial air velocities (case 1: V^S_{air} = 1 m/s; case 2: V^S_{air} = 5 m/s; case 3: V^S_{air} = 8.4 m/s) the mean value of the axial velocity increases with increasing superficial air velocities. At t = 0.4s these 3 cases mentioned a stratified flow whether it is smooth or wavy as shown in Fig. 6. This pattern explains the maintaining of an almost constant water level at the interface regardless of the increase in superficial air velocity. This statement is further observed and developed in Fig. 8. However, the fourth case (V^S_{air} = 10 m/s) refers to the slug flow configuration as already shown in Fig. 6. The run of the slug through the channel left a liquid thin film ahead (x = 15D). The high superficial air velocity (V^S_{air} = 10 m/s) creates drag forces that increase the area occupied by the air phase and reduce the liquid level. As the

surface area of the air phase has grown, the maximum air velocity shows a reduction compared to the third case.

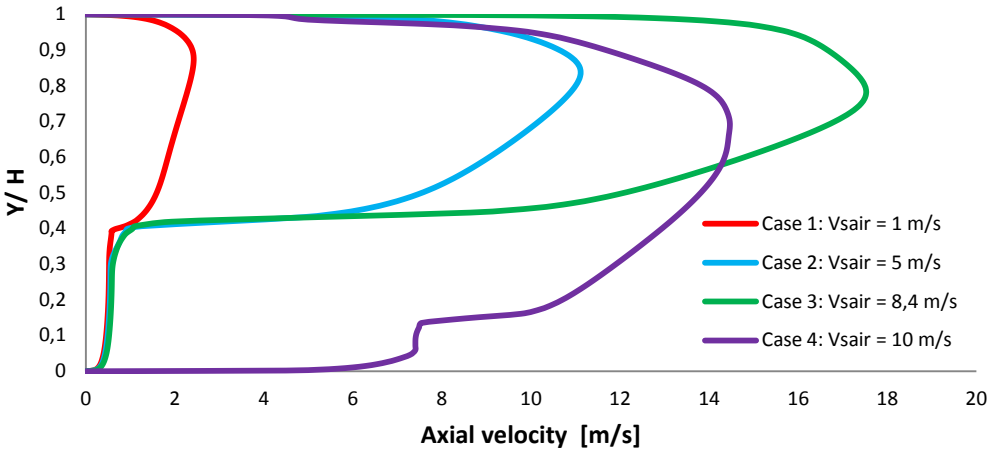

Fig.7 : Vertical profiles of the axial velocity Ux for x = 15 D in the median plane for different superficial air velocities at t=0.4s

Fig. 8 is a plot of the ratio of the liquid height and the channel height, H_L/H, vs. superficial air velocity, V^s_{air} for different axial positions in the channel (x=5D, x=10D, x=15D, x=20D). This type of plot is useful to investigate the effect of air on water level. At very low superficial air velocities (V^s_{air} < 4 m/s) the water level is insensitive to the superficial air velocity and remains approximately constant. It is mainly dependent on the location along the channel: for a constant superficial air velocity, the water level is the highest close to the inlet. Then for higher superficial air velocities V^s_{air} > 4 m/s, the liquid level became dependent to superficial air velocity and starts to decrease. This is explained by the momentum transfer between air and water which becomes important for V^s_{air} > 4 m/s thus increasing the water velocity and consequently reducing the liquid height H_L.

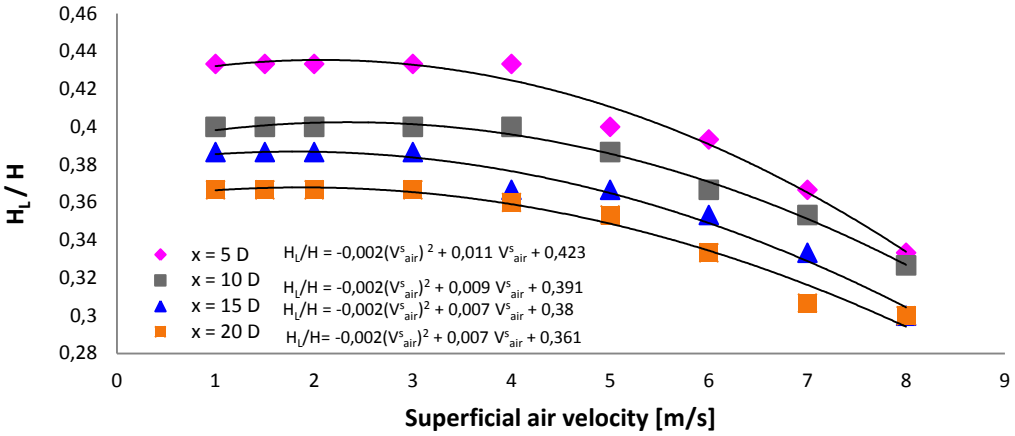

Fig.8: Water level variation as a function of superficial air velocity V^s_{air} for different axial positions

Fig. 9 shows the vertical profiles of wall shear stress for x = 10D for different superficial air velocities (V^S_{air} = 1, 5, 8.4 and 10 m/s) at t=0,4s. As can be seen, the vertical evolution of the wall shear stress has the same shape for the 3 cases where the flow is considered as stratified smooth and stratified wavy (V^S_{air} = 1, 5, and 8.4 m/s). The highest value of the wall shear stress for each case is observed at the air-water interface (y / H = 0.037). This increase can be attributed to the effect of density. For the case where the slug flow is seen (V^S_{air} = 10 m/s), the maximum value of the wall shear stress is observed at the bottom of the channel (y / H < 0.1) since the liquid level was reduced and only a thin layer is left.

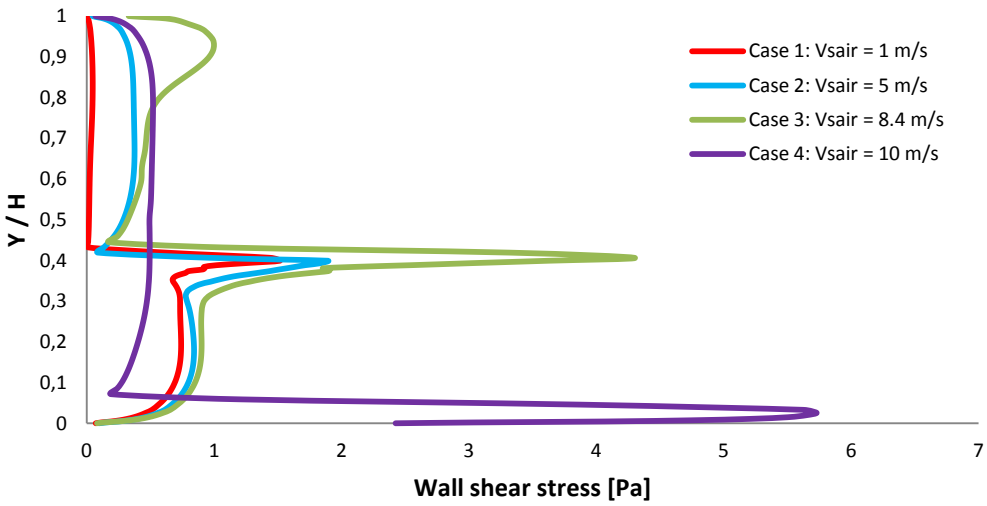

Fig.9: Vertical profiles of wall shear stress at x = 10D for different superficial air velocities at t = 0.4s

Fig. 10 presents the time evolution of the relative pressure for different superficial air velocities (V^S_{air} = 1, 5, 8.4 and 10 m/s). The pressure for cases where the superficial air velocity is equal to 1 m/s and 5 m/s is almost constant and its variation is not significant

compared to the other cases. However case 3 (V^S_{air} = 8.4 m/s) and case 4 (V^S_{air} = 10 m/s) show high pressure fluctuations. The latter two cases are the cases where a slug flow was observed. Thus, the slug regime is revealed by the sudden changes in pressure. This strong pulsation occurs once the slug hits the upper channel wall which causes its obstruction and disappears once it leaves the channel. This observation is confirmed by Fig. 11 and Fig. 12.

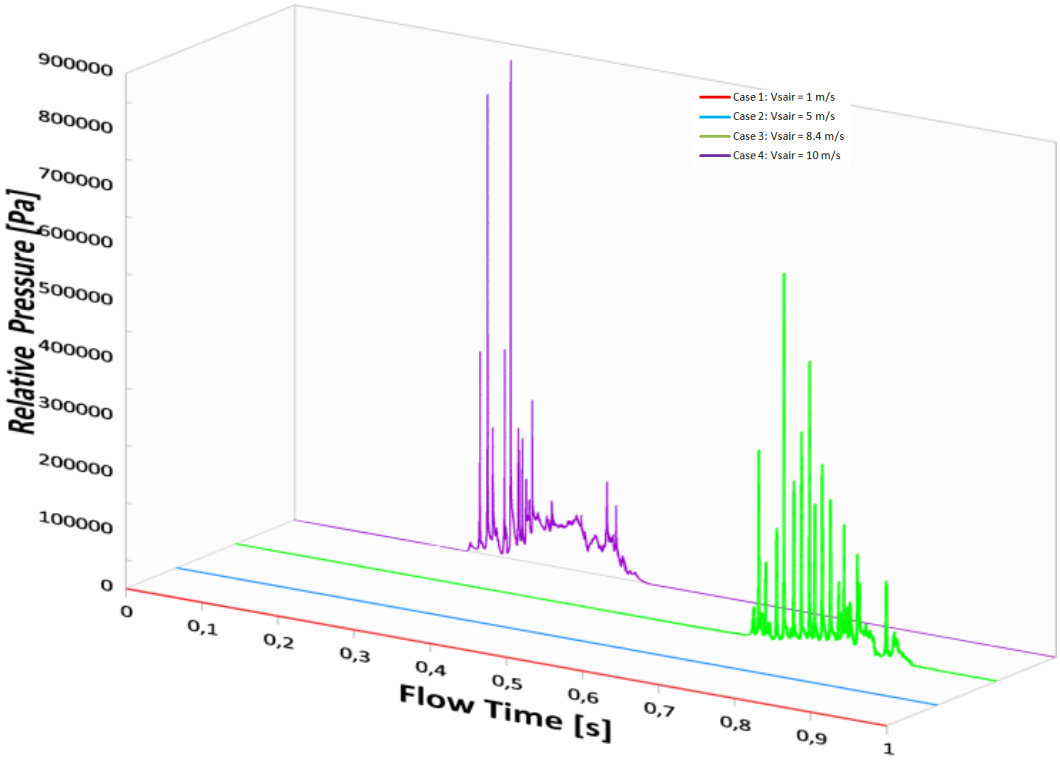

Fig. 10. Time evolution of the relative pressure for different superficial air velocities at x = 5D

Fig. 11 and Fig. 12 depict the time evolution of relative pressure for different locations x in the channel (x= 5D, x = 15D, x = 25D) for V^S_{air} = 8.4 m/s and V^S_{air} = 10 m/s, respectively. The abrupt jump in oscillation starts at t = 0.68 s and t = 0.24 s for V^S_{air} = 8.4 m/s and V^S_{air} = 10 m/s, respectively. These instants reveals the moment where the slug was created. This observation confirms the wavy flow shown in Fig. 6 for the third case (V^S_{air} = 8.4 m/s) since the plot was taken at t = 0.4s; the slug appeared only at t = 0.68s. Then at t = 0.88s and t = 0.44s for V^S_{air} = 8.4 m/s and V^S_{air} =10 m/s, respectively, the pressure decreases and remains constant. These instants indicate that the slug has left the channel. Comparing these two Figures, it is apparent that the higher the superficial air velocity is, the higher the pressure rises and the faster the slug occurs.

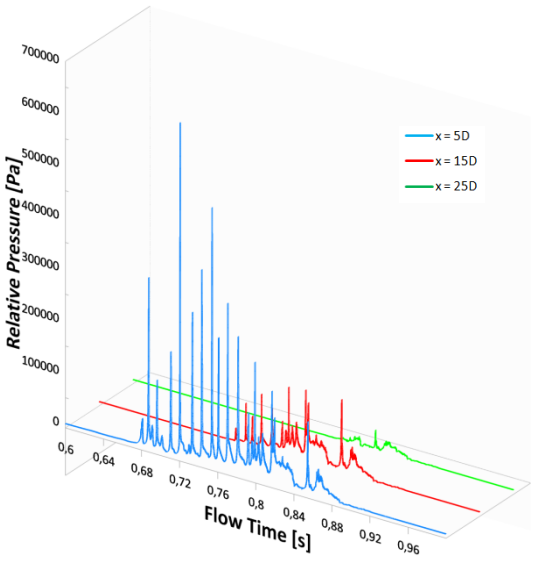

Fig. 11. Time evolution of the relative pressure for different positions x in the median plane for V^s_{air} = 8.4 m/s and V^s_{water}=0.16 m/s

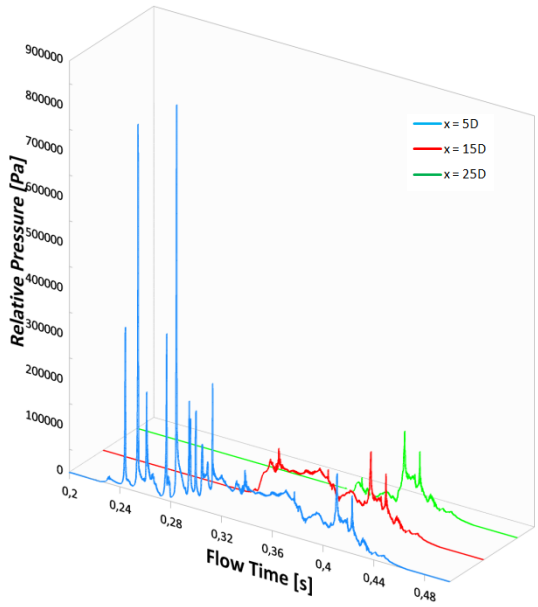

Fig. 12. Time evolution of the relative pressure for different positions x in the median plane for V^s_{air} = 10 m/s and V^s_{water}=0.16 m/s

4.4 Study of the slug occurrence

The presence of slug flow inside sewer system has the potential to obstruct the air flow above the water, and result in high pressure fluctuation that cause mechanical damage to the sewer system. Thus, it is a major of interest to provide a fundamental insight into the parameters that characterize the slug flow. We assume that the air velocity generated by vents upstream the flow governs the behavior of slugs created inside channels. For this reason, the measurement of both superficial air and water velocities inside horizontal channels is required to give an accurate prediction of the slug initiation and therefore to avoid them. Thus, this section will present results tested under four different superficial water velocities as mentioned in Table 5.

Fig. 13 illustrates the evolution of the critical superficial air velocity as a function of the superficial water velocity. Under the line plotted only stratified smooth or/and stratified wavy flow occur. The linear line plotted with a negative slope shows that as much as the superficial water velocity increases, the critical superficial air velocity decreases. This can be explained by energy transfer. It seems that the energy needed by air to raise water, is regained from the increase of water flow rate. Thus the critical air velocity is decreased. In this way, the critical superficial air velocity can be correlated as a function of superficial water velocity as follows:

$$V^s_{air} = -20.345V^s_{water} + 11.529 \quad (18)$$

Table 5 the superficial water velocities for the simulated cases

Cases	Superficial water velocity [m/s]
A	0.16
B	0.2
C	0.26
D	0.3

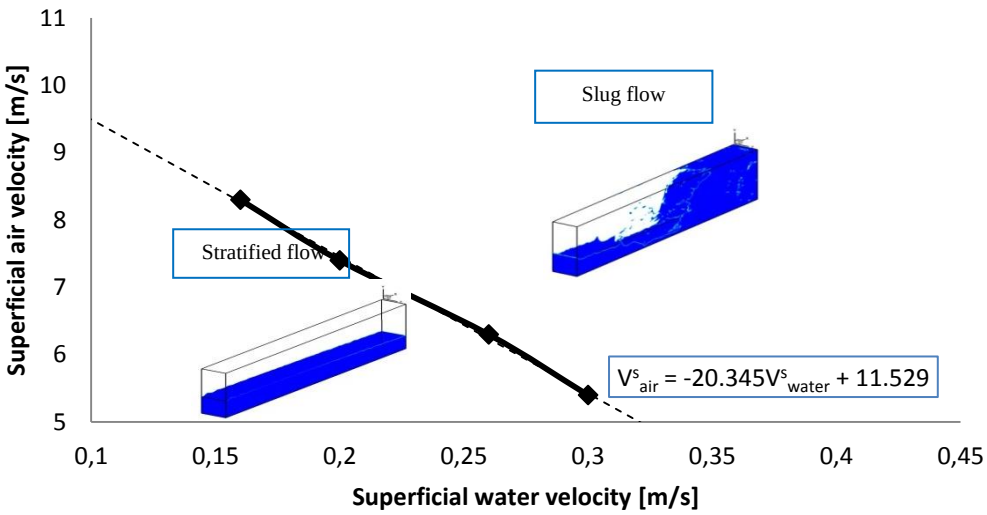

Fig. 13. Critical superficial air velocity for different superficial water velocities for a fixed inlet water level HL = 0.37 H.

For a better understanding of the slug behaviour we extracted the time occurrence of slug and its position from the channel inlet in function of superficial air velocities for three superficial water velocities while keeping the water level fixed for all cases H_L = 0.37 H.

Fig. 14 depicts the slug occurrence position X_s as a function of the superficial air velocity for different superficial water velocities. It is noticed that the effect of superficial air velocity on slug flow is significant in terms of the position of the slug inside confined channels. The slug gets closer to the channel inlet as much as the superficial air velocity increases. It shows that as the superficial air velocity increases, the slug is getting closer to the inlet. The slug occurrence position decrease may be approximated by a power law function ($X_s = A(V^s_{air})^n (V^s_{eau})^m$); where n and m are dependent on the superficial air and water velocities.

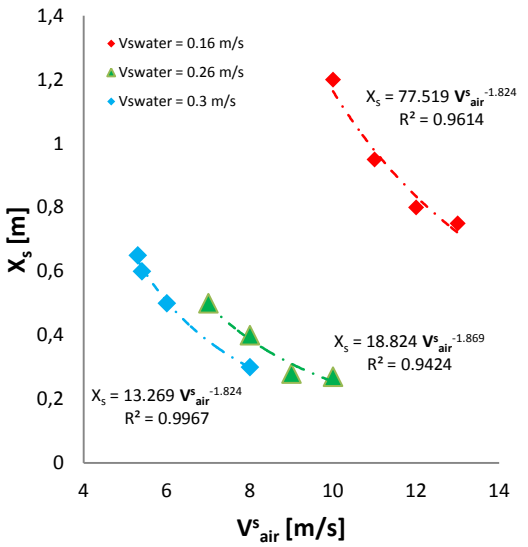

Fig. 14. Slug position occurrence as a function of superficial air velocity.

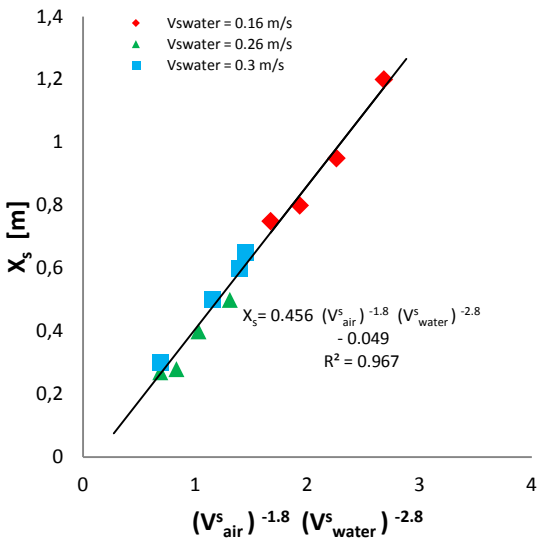

Fig. 15.Variation of Slug position occurrence Xs according to $V^s_{air}{}^{(-1.8)}$ $V^s_{water}{}^{(-2.8)}$

In Fig. 15, X_s is presented as a function of ($V^s_{air}{}^{(-1.8)}$ $V^s_{water}{}^{(-2.8)}$). As can be seen, the three curves of Fig. 14 are turned into a unique linear line with a slope of 0.45. In this way, the slug occurrence position X_s can be correlated as a function of superficial air and water velocities as follows:

$$X_s = 0.45\ (V^s_{air})^{-1.8}\ (V^s_{water})^{-2.8} \tag{19}$$

The slug occurrence position X_s decreases with both high superficial air and water velocities. Thus, the slug occurrence position X_s becomes closer to the channel inlet.

In the same spirit, and being aware of the relation between the time of slugs initiation with air and water velocities, we have shown the relationship that can link time and inlet velocities. Fig. 16 illustrates the appearance time of slug t_s as a function of the superficial air velocity for different superficial water velocities. It is noticed that the effect of superficial air velocity on slug flow is significant in terms of the time appearance of slugs inside confined channels. It's pretty clear that as superficial air velocity increases, the slug is getting faster. The appearance time of the slug decrease may be approached in the form of a power law function (t_s = A $(V^s_{air})^n$ $(V^s_{water})^m$); where n and m are depending on the superficial air and water velocities).

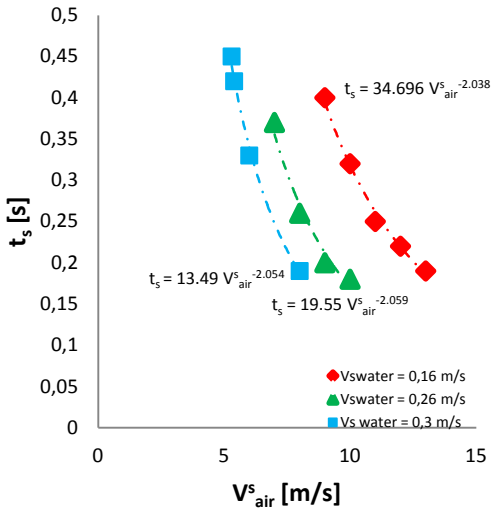

Fig. 16. Slugs Time appearance as a function of superficial air velocity for different superficial water velocities

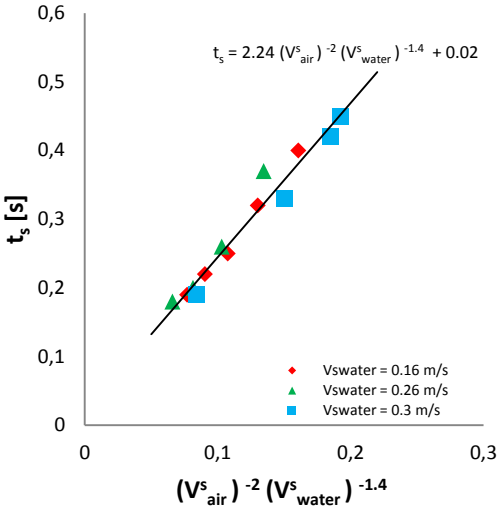

Fig. 17.Variation of Slug Time appearance t_s according to $V^s_{air}{}^{(-2)}\ V^s_{water}{}^{(-1.4)}$

In Fig. 17, t_s is plotted as a function of $V^s_{air}{}^{(-2)}\ V^s_{water}{}^{(-1.4)}$. The three curves in Fig. 16 are turned into a straight line with a slope of 2.2. Thus, the time appearance of the slug t_s can be correlated in terms of superficial air and water velocities as follows:

$$t_s = 2.2 \times (V^s_{air})^{-2}\ (V^s_{water})^{-1.4} \tag{20}$$

The time appearance of the slug decreases with both high superficial air and water velocities. Thus, the slug appearance becomes faster.

According to correlations (19) and (20), it is now possible to predict the time and the position of the slug occurrence in the channel. Hence, it could be anticipated and controlled in order to avoid the blockage phenomenon of flows inside sewer systems.

Conclusion

This paper reports a study of the slug flow occurring inside horizontal confined channel. Experimental measurements were carried out on the experimental setup of the IUSTI laboratory of the University of Aix Marseille using the LDA technique. Numerical model has been developed using the Volume Of Fluid method (VOF) to track the dynamic behavior of the air-water interface. The VOF interface model is well adapted to the prediction of two-

phase flows with strong interfacial disturbances. Numerical results of the axial velocity have shown a good agreement with the experimental data for two water levels (H_L=0.21 H and H_L=0.37 H). On the basis of the above findings, the main conclusions can be briefly summarized as follows:

- Under a constant superficial water velocity (V^s_{water}= 0.16 m/s) and a wide variation of the superficial air velocity 0.6-13 m/s. We concluded that the higher the velocity, the stronger the interface instability. Very high air superficial velocities force the waves created on the interface to rise and grow until they rich the upper wall of the channel and bridge its cross section. Waves become slugs that make significant pressure oscillations threatening the infrastructure of the channel.
- As the superficial water velocity increases, the critical superficial air velocity decreases due to the transfer of energy between the two fluids. Hence, a transition line between the stratified and the slug flow for a range of superficial water velocities set to 0.16-0.3m/s was defined (V^s_{air} = -20.345 V^s_{water} + 11.529). Such outcome represents fundamental insight into the understanding and control of two phase flow giving help and assistance to practitioners, engineers and researches in eliminating the formation of slugs inside channels therefore avoiding channel obstruction. For example, if the superficial water velocity flowing in the channel is equal to V^s_{water} = 0.3 m/s, the superficial air velocity introduced must not exceed V^s_{air} = 5.425 m/s.
- Correlations have been established in terms of the superficial air and water velocities enabling the identification of the position ($X_s = 0.45(V^s_{air})^{-1.8}(V^s_{water})^{-2.8}$) and the time of the slug formation ($t_s = 2.2(V^s_{air})^{-2}(V^s_{water})^{-1.4}$). With the suggested correlations, the position and time of the slugs occurrence inside confined channels can be rapidly and easily determined without any requirement for experimental studies or numerical simulations. Such results may be a useful tool to anticipate slug flow. Further work is in progress to find a solution to the channel blockage phenomenon by modifying the air injection mode.

References

[1] M. A. Hamam and J. A. McCorquodale, “Transient Conditions in the Transition From Gravity To Surcharged Sewer Flow.,” *Can. J. Civ. Eng.*, vol. 9, no. 2, pp. 189–196, 1982, doi: 10.1139/l82-022.

[2] J. G. Vasconcelos and S. J. Wright, “Experimental investigation of surges in a stormwater storage tunnel,” *J. Hydraul. Eng.*, vol. 131, no. 10, pp. 853–861, 2005, doi: 10.1061/(ASCE)0733-9429(2005)131:10(853).

[3] S. J. Wright, “Air – water interactions in urban drainage systems,” 2017.

[4] A. S. Leon, “Mechanisms that lead to violent geysers in vertical shafts,” *J. Hydraul. Res.*, vol. 57, no. 3, pp. 295–306, 2019, doi: 10.1080/00221686.2018.1459895.

[5] F. Zhou, F. E. Hicks, and P. M. Steffler, “□ □,” no. June, pp. 625–634, 2002.

[6] F. Zhou, F. Hicks, and P. Steffler, “Analysis of effects of air pocket on hydraulic failure of urban drainage infrastructure,” *Can. J. Civ. Eng.*, vol. 31, no. 1, pp. 86–94, 2004, doi: 10.1139/l03-077.

[7] L. Zhou, D. Liu, and B. Karney, “Investigation of hydraulic transients of two entrapped air pockets in a water pipeline,” *J. Hydraul. Eng.*, vol. 139, no. 9, pp. 949–959, 2013, doi: 10.1061/(ASCE)HY.1943-7900.0000750.

[8] J. G. Vasconcelos and S. J. Wright, “Anticipating transient problems during the rapid filling of deep stormwater storage tunnel systems,” *J. Hydraul. Eng.*, vol. 143, no. 3, pp. 1–8, 2017, doi: 10.1061/(ASCE)HY.1943-7900.0001250.

[9] F. Granata, G. de Marinis, and R. Gargano, “Air-water flows in circular drop manholes,” *Urban Water J.*, vol. 12, no. 6, pp. 477–487, 2015, doi: 10.1080/1573062X.2014.881893.

[10] Y. Eldayih, M. Cetin, and J. G. Vasconcelos, “Air-Pocket Entrapment Caused by Shear Flow Instabilities in Rapid-Filling Pipes,” *J. Hydraul. Eng.*, vol. 146, no. 4, 2020, doi: 10.1061/(ASCE)HY.1943-7900.0001711.

[11] J. G. Vasconcelos and S. J. Wright, “Geysering generated by large air pockets released through water-filled ventilation shafts,” *J. Hydraul. Eng.*, vol. 137, no. 5, pp. 543–555, 2011, doi: 10.1061/(ASCE)HY.1943-7900.0000332.

[12] J. G. Vasconcelos, P. R. Klaver, and D. J. Lautenbach, “Flow regime transition simulation incorporating entrapped air pocket effects,” *Urban Water J.*, vol. 12, no. 6, pp. 488–501, 2015, doi: 10.1080/1573062X.2014.881892.

[13] P. Taylor *et al.*, “Failure of a drainage tunnel caused by an entrapped air pocket,” no. June 2015, pp. 37–41, doi: 10.1080/1573062X.2015.1041990.

[14] A. Z. Hudaya, H. Y. Kuntoro, O. Dinaryanto, Deendarlianto, and Indarto, “Experimental investigation on the interfacial characteristics of stratified air-water two-phase flow in a horizontal pipe,” *AIP Conf. Proc.*, vol. 1737, 2016, doi: 10.1063/1.4949300.

[15] O. Dinaryanto *et al.*, “Experimental investigation on the initiation and flow development of gas-liquid slug two-phase flow in a horizontal pipe,” *Exp. Therm. Fluid Sci.*, vol. 81, pp. 93–108, 2017, doi: 10.1016/j.expthermflusci.2016.10.013.

[16] R. Kong, A. Rau, S. Kim, S. Bajorek, K. Tien, and C. Hoxie, “Experimental study of horizontal air-water plug-to-slug transition flow in different pipe sizes,” *Int. J. Heat Mass Transf.*, vol. 123, pp. 1005–1020, 2018, doi: 10.1016/j.ijheatmasstransfer.2018.03.027.

[17] B. Bae, T. Ahn, J. Jeong, K. Kim, and B. Yun, “Characteristics of an interfacial wave in a horizontal air-water stratified flow,” *Int. J. Multiph. Flow*, vol. 97, pp. 197–205, 2017, doi: 10.1016/j.ijmultiphaseflow.2017.08.009.

[18] C. Vallee, T. Hohne, H.-M. Prasser, and T. Suhnel, “{E}xperimental investigation and {CFD} simulation of slug flow in horizontal channels,” no. FZD-485, pp. 95–103, 2007.

[19] C. Vallée, T. Höhne, H. M. Prasser, and T. Sühnel, “Experimental investigation and CFD simulation of

horizontal stratified two-phase flow phenomena," *Nucl. Eng. Des.*, vol. 238, no. 3, pp. 637–646, 2008, doi: 10.1016/j.nucengdes.2007.02.051.

[20] P. Vollestad, A. A. Ayati, L. Angheluta, J. H. LaCasce, and A. Jensen, "Experimental investigation of airflow above waves in a horizontal pipe," *Int. J. Multiph. Flow*, vol. 110, pp. 37–49, 2019, doi: 10.1016/j.ijmultiphaseflow.2018.08.008.

[21] A. Z. Hudaya, A. Widyatama, O. Dinaryanto, W. E. Juwana, Indarto, and Deendarlianto, "The liquid wave characteristics during the transportation of air-water stratified co-current two-phase flow in a horizontal pipe," *Exp. Therm. Fluid Sci.*, vol. 103, no. July 2018, pp. 304–317, 2019, doi: 10.1016/j.expthermflusci.2019.01.021.

[22] R. Kong and S. Kim, "Characterization of horizontal air–water two-phase flow," *Nucl. Eng. Des.*, vol. 312, pp. 266–276, 2017, doi: 10.1016/j.nucengdes.2016.06.016.

[23] G. Liu and Y. Wang, "Study on the natural frequencies of pipes conveying gas-liquid two-phase slug flow," *Int. J. Mech. Sci.*, vol. 141, pp. 168–188, 2018, doi: 10.1016/j.ijmecsci.2018.03.040.

[24] A. A. Ayati, J. Kolaas, A. Jensen, and G. W. Johnson, "PIV in stratified gas-liquid flow in a horizontal pipe using water droplets as tracers in the gas-phase," pp. 1–20, 2017, [Online]. Available: http://arxiv.org/abs/1701.00387.

[25] A. A. Ayati, J. Kolaas, A. Jensen, and G. W. Johnson, "Combined simultaneous two-phase PIV and interface elevation measurements in stratified gas/liquid pipe flow," *Int. J. Multiph. Flow*, vol. 74, pp. 45–58, 2015, doi: 10.1016/j.ijmultiphaseflow.2015.03.024.

[26] A. A. Ayati, J. Kolaas, A. Jensen, and G. W. Johnson, "The effect of interfacial waves on the turbulence structure of stratified air/water pipe flow," *Int. J. Multiph. Flow*, vol. 78, pp. 104–116, 2016, doi: 10.1016/j.ijmultiphaseflow.2015.09.007.

[27] A. A. Ayati and J. N. E. Carneiro, "Statistical characterization of interfacial waves in turbulent stratified gas-liquid pipe flows," *Int. J. Multiph. Flow*, vol. 103, pp. 94–105, 2018, doi: 10.1016/j.ijmultiphaseflow.2018.02.011.

[28] A. A. Ayati, P. S. C. Farias, L. F. A. Azevedo, and I. B. de Paula, "Characterization of linear interfacial waves in a turbulent gas-liquid pipe flow," *Phys. Fluids*, vol. 29, no. 6, 2017, doi: 10.1063/1.4985717.

[29] M. Olbrich, E. Schmeyer, M. Bär, M. Sieber, K. Oberleithner, and S. Schmelter, "Jo na l P," *Flow Meas. Instrum.*, p. 101814, 2020, doi: 10.1016/j.flowmeasinst.2020.101814.

[30] S. Schmelter, M. Olbrich, and E. Schmeyer, "Numerical simulation , validation , and analysis of two-phase slug flow in large horizontal pipes," vol. 73, 2020, doi: 10.1016/j.flowmeasinst.2020.101722.

[31] O. Cazarez-candia, O. C. Benítez-centeno, and I. Mexicano, "Comprehensive experimental study of liquid-slug length and Taylor-bubble velocity in slug flow," *Flow Meas. Instrum.*, vol. 72, no. June 2019, p. 101697, 2020, doi: 10.1016/j.flowmeasinst.2020.101697.

[32] S. C. K. De Schepper, G. J. Heynderickx, and G. B. Marin, "CFD modeling of all gas-liquid and vapor-liquid flow regimes predicted by the Baker chart," *Chem. Eng. J.*, vol. 138, no. 1–3, pp. 349–357, 2008, doi: 10.1016/j.cej.2007.06.007.

[33] R. Dabirian, A. Mansouri, R. Mohan, O. Shoham, and G. Kouba, "CFD simulation of turbulent flow structure in stratified gas/liquid flow and validation with experimental data," *Proc. - SPE Annu. Tech. Conf. Exhib.*, vol. 2015-Janua, pp. 3291–3306, 2015, doi: 10.2118/174964-ms.

[34] H. Nasrfard, H. Rahimzadeh, A. Ahmadpour, and E. Amani, "Simulation of Intermittent Flow Development in a Horizontal Pipe," *J. Fluids Eng. Trans. ASME*, vol. 141, no. 12, pp. 1–10, 2019, doi: 10.1115/1.4044069.

[35] C. A. S. Costa, P. M. de Oliveira, and J. R. Barbosa, "Intermittent flow initiation in a horizontal tube: quantitative visualization and CFD analysis," *J. Brazilian Soc. Mech. Sci. Eng.*, vol. 40, no. 4, 2018, doi: 10.1007/s40430-018-1124-6.

[36] W. P. R. B. M. Norpiah, M. S. Nasif, B. Sam, "NUMERICAL VALIDATION OF GAS-LIQUID SLUG FLOW INSIDE HORIZONTAL PIPE," *J. Fundam. Appl. Sci.*, 2017, doi: http://dx.doi.org/10.4314/jfas.v9i5s.46.

[37] M. R. Ansari and V. Shokri, "Numerical modeling of slug flow initiation in a horizontal channels using a two-fluid model," *Int. J. Heat Fluid Flow*, vol. 32, no. 1, pp. 145–155, 2011, doi: 10.1016/j.ijheatfluidflow.2010.09.002.

[38] R. I. Issa and M. H. W. Kempf, "Simulation of slug flow in horizontal and nearly horizontal pipes with the two-fluid model," *Int. J. Multiph. Flow*, vol. 29, no. 1, pp. 69–95, 2003, doi: 10.1016/S0301-9322(02)00127-1.

[39] S. Miao, K. Hendrickson, and Y. Liu, "Slug generation processes in co-current turbulent-gas/laminar-liquid flows in horizontal channels," *J. Fluid Mech.*, vol. 860, pp. 224–257, 2019, doi: 10.1017/jfm.2018.868.

[40] U. Kadri, R. F. Mudde, R. V. A. Oliemans, M. Bonizzi, and P. Andreussi, "Prediction of the transition from stratified to slug flow or roll-waves in gas-liquid horizontal pipes," *Int. J. Multiph. Flow*, vol. 35, no. 11, pp. 1001–1010, 2009, doi: 10.1016/j.ijmultiphaseflow.2009.07.002.

[41] G. Chinello, A. A. Ayati, D. McGlinchey, G. Ooms, and R. Henkes, "Comparison of computational fluid dynamics simulations and experiments for stratified air-water flows in pipes," *J. Fluids Eng. Trans. ASME*, vol. 141, no. 5, 2019, doi: 10.1115/1.4041667.

[42] W. H. Finlay, *The Mechanics of Inhaled Pharmaceutical Aerosols*. 2019.

[43] C. Tzotzi and N. Andritsos, "Interfacial shear stress in wavy stratified gas-liquid flow in horizontal pipes," *Int. J. Multiph. Flow*, vol. 54, pp. 43–54, 2013, doi: 10.1016/j.ijmultiphaseflow.2013.03.003.

[44] M. P. Joel H. Ferziger, *Computarional Methods for Fluid Dynamics*. Springer Berlin Heidelberg, 2002.

[45] D. Choudhury, "Introduction to the Renormalization Group Method and Turbulence Modeling," *Fluent Inc Tech. Memo. TM-107*, 1993.

[46] R. Banerjee and K. M. Isaac, "IMECE2003-4 2670," pp. 1–17, 2018.

[47] N. Koutsourakis, J. G. Bartzis, and N. C. Markatos, "Evaluation of Reynolds stress, k-ε and RNG k-ε turbulence models in street canyon flows using various experimental datasets," *Environ. Fluid Mech.*, vol. 12, no. 4, pp. 379–403, 2012, doi: 10.1007/s10652-012-9240-9.

[48] M. M. Hussein, A. Al-Sarkhi, H. M. Badr, and M. A. Habib, *CFD modeling of liquid film reversal of two-phase flow in vertical pipes*, vol. 9, no. 4. Springer International Publishing, 2019.

[49] M. B. Alberto, F. O. Jesús Manuel, and M. F. Andrés, "Numerical methodology for the CFD simulation of diaphragm volumetric pumps," *Int. J. Mech. Sci.*, vol. 150, pp. 322–336, 2019, doi: 10.1016/j.ijmecsci.2018.10.039.

[50] Y. Qi, Y. Wang, and J. Zhang, "Three-dimensional turbulence numerical simulation of flow in a stepped dropshaft," *Water (Switzerland)*, vol. 11, no. 1, 2018, doi: 10.3390/w11010030.

[51] B. E. L. and D. B. Spalding, *Lectures in Mathematical Models of Turbulence*. 1972.

[52] and J. Z. T.-H. Shih, W. W. Liou, A. Shabbir, Z. Yang, "A New k-_ Eddy- Viscosity Model for High Reynolds Number Turbulent Flows - Model Development and Validation," *Comput. Fluids*, vol. 24(3), pp. 227–238, 1995.

[53] B. D. Hirt, C.W.; Nichols, "Volume of fluid (VOF) method for the dynamics of free boundaries," *J. Comput. Phys.*, vol. 39, pp. 201–225, 1981.

[54] H. Mahmoud, W. Kriaa, H. Mhiri, G. Le Palec, and P. Bournot, "A numerical study of a turbulent axisymmetric jet emerging in a co-flowing stream," *Energy Convers. Manag.*, vol. 51, no. 11, pp. 2117–2126, 2010, doi: 10.1016/j.enconman.2010.03.004.

Figure Captions List

Fig.1. a. Photograph of the experimental setup of the IUSTI, b. Schematic diagram of the experimental setup
Fig.2: a. Generated mesh grid for the channel, b. Mesh grid of the channel wall, c. Mesh grid of the channel inlet (air inlet and water inlet section)
Fig.3: Vertical profiles of the axial velocity U_x at x = 41 D in the median plane for HL = 0.21 H.
Fig.4: Vertical profiles of the axial velocity U_x for x = 41 D in the median plane at HL = 0.21 H
Fig.5: Vertical profiles of the axial velocity for x = 41 D in the median plan at HL = 0.37 H
Fig.6: Contours of volume fraction in the median plane for air-water flow for different superficial air velocities at t = 0.4 s
Fig.7 : Vertical profiles of the axial velocity Ux for x = 15 D in the median plane for different superficial air velocities at t=0.4s
Fig.8: Water level variation as a function of superficial air velocity V^s_{air} for different axial positions
Fig.9: Vertical profiles of wall shear stress at x = 10D for different superficial air velocities at t = 0.4s
Fig. 10. Time evolution of the relative pressure for different superficial air velocities at x = 5D
Fig. 11. Time evolution of the relative pressure for different positions x in the median plane for V^s_{air} = 8.4 m/s and V^s_{water}=0.16 m/s
Fig. 12. Time evolution of the relative pressure for different positions x in the median plane for V^s_{air} = 10 m/s and V^s_{water}=0.16 m/s
Fig. 13. Critical superficial air velocity for different superficial water velocities for a fixed inlet water level HL = 0.37 H.
Fig. 14. Slug position occurrence as a function of superficial air velocity.
Fig. 15.Variation of Slug position occurrence Xs according to $V^s_{air}{}^{(-1.8)}$ $V^s_{water}{}^{(-2.8)}$
Fig. 16. Slugs Time appearance as a function of superficial air velocity for different superficial water velocities
Fig. 17.Variation of Slug Time appearance t_s according to $V^s_{air}{}^{(-2)}$ $V^s_{water}{}^{(-1.4)}$